








## RESEARCH ARTICLE

# Using spectral diversity and heterogeneity measures to map habitat mosaics: An example from the Classical Karst

Emilia Pafumi<sup>1,2,3</sup>  | Francesco Petruzzellis<sup>1</sup>  | Miris Castello<sup>1</sup>  | Alfredo Altobelli<sup>1</sup>  |  
Simona Maccherini<sup>2,3</sup>  | Duccio Rocchini<sup>4,5</sup>  | Giovanni Bacaro<sup>1</sup> 

<sup>1</sup>Department of Life Sciences, University of Trieste, Trieste, Italy

<sup>2</sup>Department of Life Sciences, University of Siena, Siena, Italy

<sup>3</sup>NBFC, National Biodiversity Future Center, Palermo, Italy

<sup>4</sup>BIOME Lab, Department of Biological, Geological and Environmental Sciences, Alma Mater Studiorum University of Bologna, Bologna, Italy

<sup>5</sup>Faculty of Environmental Sciences, Department of Spatial Sciences, Czech University of Life Sciences Prague, Praha – Suchbátka, Czech Republic

## Correspondence

Emilia Pafumi, Department of Life Sciences, University of Siena, Via P.A. Mattioli 4, 53100 Siena, Italy.  
Email: [e.pafumi@student.unisi.it](mailto:e.pafumi@student.unisi.it)

## Funding information

Rural Development Program (Programma di Sviluppo Rurale) 2014–2020 of Friuli Venezia Giulia Region; Italian Ministry of University (MUR)

**Co-ordinating Editor:** Sebastian Schmidtlein

## Abstract

**Questions:** Can we map complex habitat mosaics from remote-sensing data? In doing this, are measures of spectral heterogeneity useful to improve image classification performance? Which measures are the most important? How can multitemporal data be integrated in a robust framework?

**Location:** Classical Karst (NE Italy).

**Methods:** First, a habitat map was produced from field surveys. Then, a collection of 12 monthly Sentinel-2 images was retrieved. Vegetation and spectral heterogeneity (SH) indices were computed and aggregated in four combinations: (1) monthly layers of vegetation and SH indices; (2) seasonal layers of vegetation and SH indices; (3) yearly layers of SH indices computed across the months; and (4) yearly layers of SH indices computed across the seasons. For each combination, a Random Forest classification was performed, first with the complete set of input layers and then with a subset obtained by recursive feature elimination. Training and validation points were independently extracted from field data.

**Results:** The maximum overall accuracy (0.72) was achieved by using seasonally aggregated vegetation and SH indices, after the number of vegetation types was reduced by aggregation from 26 to 11. The use of SH measures significantly increased the overall accuracy of the classification. The spectral  $\beta$ -diversity was the most important variable in most cases, while the spectral  $\alpha$ -diversity and Rao's Q had a low relative importance, possibly because some habitat patches were small compared to the window used to compute the indices.

**Conclusions:** The results are promising and suggest that image classification frameworks could benefit from the inclusion of SH measures, rarely included before. Habitat mapping in complex landscapes can thus be improved in a cost- and time-effective way, suitable for monitoring applications.

## KEYWORDS

biodiversity, multitemporal classification, Random Forest, Sentinel-2, spectral diversity, spectral heterogeneity, vegetation indices, vegetation mapping

This is an open access article under the terms of the [Creative Commons Attribution](https://creativecommons.org/licenses/by/4.0/) License, which permits use, distribution and reproduction in any medium, provided the original work is properly cited.

© 2023 The Authors. *Applied Vegetation Science* published by John Wiley & Sons Ltd on behalf of International Association for Vegetation Science.

## 1 | INTRODUCTION

Mapping natural habitats is fundamental for the conservation of biodiversity. The Habitats Directive (European Commission, 1992) requires EU member states to conserve habitats and species “of community interest” and to assess their conservation status every six years, by reporting on parameters such as habitat area, range, indicators of habitat quality and future provisions for habitat survival (European Commission, 2005). These reports require regular habitat mapping. However, habitat maps are traditionally produced through time-consuming and costly field surveys, making them unsuitable for regular updates. Thus, more cost- and time-effective monitoring strategies are required, and remote sensing has high potential to become an essential tool (Corbane et al., 2015).

Habitat mapping by remote sensing is generally carried out through automatic image classification, in which all pixels in an image are categorized into classes (Borra et al., 2019). Over time, many data sources have become available, while image-processing tools have been improved, allowing a broad range of habitats to be mapped (Corbane et al., 2015). Despite these advances, some types of habitats remain difficult to map, especially in heterogeneous areas. Mosaics of grassland types, for example, are particularly challenging to map, due to the small spatial extent of the habitat patches, their spectral similarity, and the high spatial, structural and temporal variability of the vegetation (Corbane et al., 2015). Moreover, boundaries between the patches are often not discrete (Rocchini et al., 2013). Thus, innovative approaches should be tested (Schuster et al., 2015).

Multitemporal data facilitate the differentiation of habitats in areas with seasonal variability, based on the phenological differences among vegetation types (Rapinel et al., 2019). However, there are many ways to include the multitemporal information in the classification process: increasing the number of images (Schuster et al., 2015), using a time series of a single vegetation index (Tarantino et al., 2021), or using seasonal composites (Praticò et al., 2021).

Image classifications can also be improved by ancillary data, such as topographic features, that influence the distribution of natural communities on fine scales (Bhatt et al., 2022), and data on vegetation structure derived from active sensors (Osińska-Skotak et al., 2021). However, some of the greatest improvements are achieved when texture information is included (Khatami et al., 2016). Image texture metrics measure the spatial arrangement and variation of pixel values, and thus provide valuable information on the homogeneity of areas (Haralick et al., 1973).

The spatial variability of the remotely sensed signal is also the basis for the assessment of plant biodiversity from remote sensing (Rocchini, Balkenhol, et al., 2010). The spectral diversity, or spectral heterogeneity (SH), has been directly related to environmental heterogeneity (Spectral Variation Hypothesis; Palmer et al., 2002), and is often positively related to species

diversity (Rocchini, Balkenhol, et al., 2010). The relationship between SH and species diversity is not universally valid (Fassnacht et al., 2022), since it is sensitive to spatial scale (Wang et al., 2018), spectral resolution (Rossi et al., 2021) and temporal scale (Fauvel et al., 2020). However, SH can be useful regardless of its relationship with taxonomic diversity, since it integrates a broad range of vegetation properties and their spatial arrangement (Wang & Gamon, 2019).

Among the many measures of SH, two novel approaches have emerged (Wang & Gamon, 2019). The first one relies on information theory: diversity indices based on information theory, such as Rao's quadratic entropy, are computed from spectral data, generally by applying the moving-window approach (Rocchini, Marcantonio, et al., 2021). The second approach is based on “spectral species,” that is, spectral types considered as proxies for biological species (Féret & Asner, 2014). Following this approach, each pixel of the image is assigned to a spectral species, and metrics of  $\alpha$ - and  $\beta$ -diversity are inferred from the variation in spectral species (Féret & de Boissieu, 2020). So far, this method has been applied to tropical forests, based on very high-resolution airborne imaging spectroscopy (2 m/pixel; Féret & Asner, 2014), to low-resolution MODIS images of Europe (500 m/pixel; Rocchini, Salvatori, et al., 2021), and recently also to Sentinel-2 data (10 m/pixel), in secondary forests (Chraïbi et al., 2021) and in an ecological network (Licari et al., 2022).

In this light, measures of SH have the potential to improve habitat mapping frameworks, especially in complex landscape mosaics. Indeed, when vegetation types share similar spectral reflectance characteristics, considering additional levels of information may facilitate their differentiation (Bhatt et al., 2022). The variability of taxonomic, functional and phylogenetic traits, as expressed by SH, may be such a type of information (Wang & Gamon, 2019). However, very few studies have tried to incorporate these measures for habitat mapping (e.g. Marzialetti et al., 2020).

Moving forward from these premises, the aim of this study was to test and discuss an integrated approach to map a complex mosaic of natural and semi-natural habitats through remote sensing, using the Classical Karst as a case study. The habitats considered correspond to the main vegetation types present in the study area. Specifically, the main objectives were:

1. to quantify the importance of measures of SH for habitat classification;
2. to provide a robust framework to include multitemporal remotely sensed data for habitat classification.

To achieve these goals, multiple sets of remote-sensing-derived variables, namely vegetation and SH indices, were computed based on a series of Sentinel-2 images and aggregated in four combinations, for which separate classifications were performed. Classification accuracies were compared to find the most reliable approach.

## 2 | METHODS

### 2.1 | Study area

The study was carried out in the Italian part of the Classical Karst, a limestone plateau with altitudes ranging from 0 to 600m, located in the provinces of Trieste and Gorizia (NE Italy; [Figure 1](#)). Six different areas involved in a habitat restoration project called “Ecomosaico del Carso” were considered, for a total surface of 55 ha (see [Table S1](#) for details). These areas are partially included in two Natura-2000 network sites: the special area of conservation “Carso Triestino e Goriziano” (IT3340006) and the special protection area “Aree carsiche della Venezia Giulia” (IT3341002).

Land cover is a fine mosaic of natural and semi-natural habitats, where the main vegetation types are grasslands, downy oak (*Quercus pubescens*) woodland and black pine (*Pinus nigra*) plantations. The Karst grassland is an extremely species-rich herbaceous formation dominated by grasses that evolved through thousands of years of grazing and is now being replaced by shrublands and woodlands due to land use abandonment. Downy oak woodlands are expanding in abandoned pastures and cover 70% of the Karst nowadays. Black pine has been introduced since the mid-19th century for reforestation purposes resulting in extensive species-poor pine plantations and from then on it has spontaneously expanded (Poldini, 1989, 2009). Many conservation

projects are being developed to maintain and restore Karst grasslands (Marin & Altobelli, 2021), which are recognized as habitats of community interest [code 62A0 “Eastern sub-Mediterranean dry grasslands (*Scorzoneratalia villosae*)” included in Annex I of the Habitats Directive].

The climate of the study area is transitional between Mediterranean and continental (Poldini, 1989), with an average rainfall of 1200mm/year, and a mean annual temperature of 12.5°C, but with large differences due to elevation and slope exposure (OSMER, 2015).

### 2.2 | Field data collection

Field surveys were carried out between March and May 2022. Habitats in the intervention areas of the “Ecomosaico del Carso” project were identified in the field. Two classifications with different degrees of detail were used to categorize the habitats. In a first classification, habitats were described as vegetation types with a high level of detail, mainly on a phytosociological basis and in most cases at the association level, according to the typologies recognized for the Classical Karst by Poldini (1989, 2009). In a second classification, habitats were classified on the basis of their structural-physiognomic and ecological features, and some classes of the first classification were aggregated into coarser types, which are the most relevant in terms of environmental conservation and management of the study

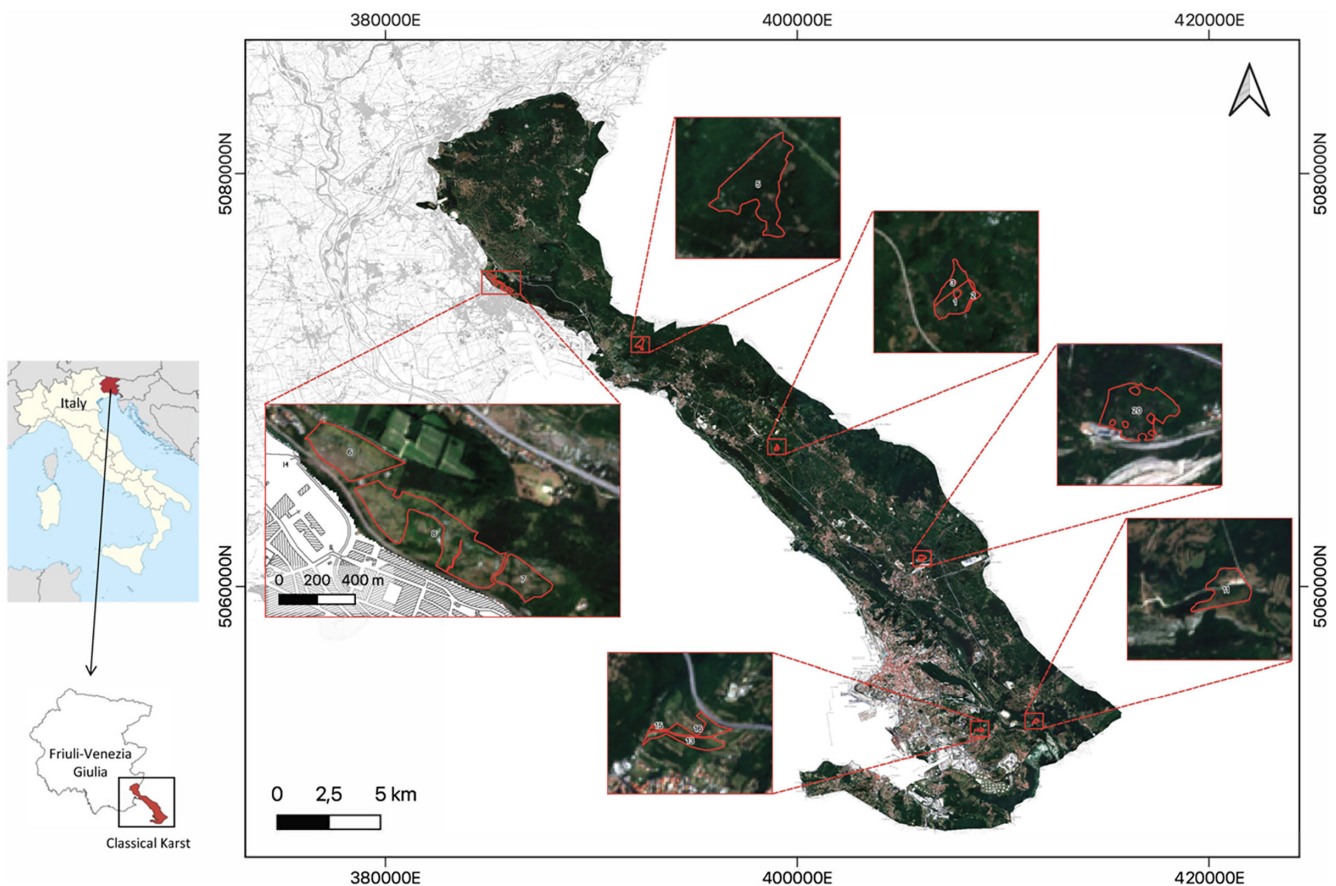


**FIGURE 1** Location of the study area in the Italian part of the Classical Karst, represented on the Sentinel-2 median composite of summer 2021. The areas involved in the “Ecomosaico del Carso” project are indicated in red.

area. The two classifications account respectively for 26 and 11 habitat classes. Specifically, for the first classification process, different classes of Karst grassland were distinguished according to the following criteria:

1. type of grassland: thermophilous calcareous, mesophilous calcareous, thermophilous on flysch;
2. degree of alteration of the floristic composition due to the presence of *Sesleria autumnalis* ("felting"), which is a species typical of scrubs and mixed oak woodlands of the Karst, its presence indicating degraded Karst grasslands or initial phases of shrub encroachment: typical grassland (rich in *Bromopsis erecta*, no *S. autumnalis*), first degradation stage (few, scattered patches of *S. autumnalis*), second degradation stage (mosaic with ca. 50% patches of typical Karst grassland and 50% *S. autumnalis*-dominated patches), third degradation stage (felted grassland, completely invaded by *S. autumnalis*);
3. dynamic stage of bush encroachment: no bushes (zero encroachment level, E0), few bushes with low height (ca < 1.5 m) and widely spaced (first encroachment level, E1), medium-height bushes (ca 3–4 m) relatively close to each other (second encroachment level, E2).

In the second classification, Karst grasslands were categorized in three classes adopting only the last criterion (bush encroachment). All shrublands distinguished in the first classification were aggregated into a single class, and the two classes of downy oak woodland – namely a class corresponding to young stages with low height individuals, and a class including mature stages with individuals higher than 6 m – were also merged. Groves with *Ailanthus altissima* and *Robinia pseudoacacia* were aggregated into an invasive alien species class, while sessile oak woodlands, black pine plantations, hay meadows and pasture grasslands were kept as separate classes. Finally, a grassland–woodland mosaic, defined as a dynamic stage with patches of grassland and well-spaced patches of downy oak woodland, was used in both classifications. The list of habitat classes considered in this study is presented in [Table S2](#).

Habitat maps were produced by field mapping for both the classifications using QGIS 3.16.14 software (QGIS Development Team, 2022). To improve the accuracy of manual mapping, we used vegetation height maps derived from LiDAR data following the procedure described in [Appendix S1](#).

### 2.3 | Satellite data collection and processing

The workflow applied to manage satellite data is given in [Figure 2](#). First, Sentinel-2 images covering the period March 2021–February 2022 were retrieved using the Google Earth Engine platform (Gorelick et al., 2017). The Sentinel-2 level-2A image collection ("COPERNICUS/S2\_SR\_HARMONIZED") was filtered by date (from March 1, 2021 to February 28, 2022), by area (the Trieste and Gorizia

Karst) and by cloud coverage (cloudy pixel percentage < 50%). The less cloudy image of each month was manually selected, to produce a collection of 12 monthly images.

Then, the 12 Sentinel-2 images were divided into four groups: spring (March–May 2021), summer (June–August 2021), autumn (September–November 2021), and winter (December 2021–February 2022). Each group was reduced to a single image by computing the median of each spectral band, so that, at each location in the output image, the pixel value of a band is the median of all pixel values of that band in the input group.

### 2.4 | Vegetation and spectral heterogeneity indices

Four vegetation indices ([Table 1](#)) were computed from each image in the monthly data set and then aggregated into seasonal median composites, following the procedure used for Sentinel-2 bands.

Rao's Q layers were separately obtained from each vegetation index raster using the R package *rasterdiv* (Thouverai et al., 2021). Then, Rao's Q was computed over the temporal dimension, producing a single raster per year, where distances among pixel values represent also the variability over time. Specifically, two sets of rasters were obtained: a set of yearly aggregated Rao's Q values computed over months, and a set of yearly aggregated Rao's Q values computed over seasons.

Spectral  $\alpha$ - and  $\beta$ -diversity layers were separately calculated from each Sentinel-2 monthly and seasonal image using the R package *biodivMapR* (Féret & de Boissieu, 2020). Then,  $\alpha$ - and  $\beta$ -diversity were computed over the temporal dimension, starting from a stack of vegetation index layers instead of a stack of spectral bands. In this way, two sets of rasters were obtained: a set of yearly aggregated  $\alpha$ - and  $\beta$ -diversity values computed over months, and a set of yearly aggregated  $\alpha$ - and  $\beta$ -diversity values computed over seasons.

All SH indices were computed in R 4.1.0 software (R Core Team, 2022). Details are in [Appendix S2](#).

### 2.5 | Satellite image classification

The remote-sensing variables were aggregated in four combinations ([Table 2](#)), that were used as input for distinct classifications.

Reference data were randomly derived from the map of habitats produced by field surveys. Training points were extracted from a set of training areas selected in the field, while validation points were launched in the whole set of polygons after excluding the training areas. Thus, training and validation points can be considered as independent. All image classifications were performed twice, first setting the number of habitat classes to 26 and then to 11, as outlined in [Section 2.2](#).

Random Forest (RF) classifications (Breiman, 2001) were performed with the *caret* R package (Kuhn, 2021). For each combination, two alternative pathways were followed. In one case, the whole

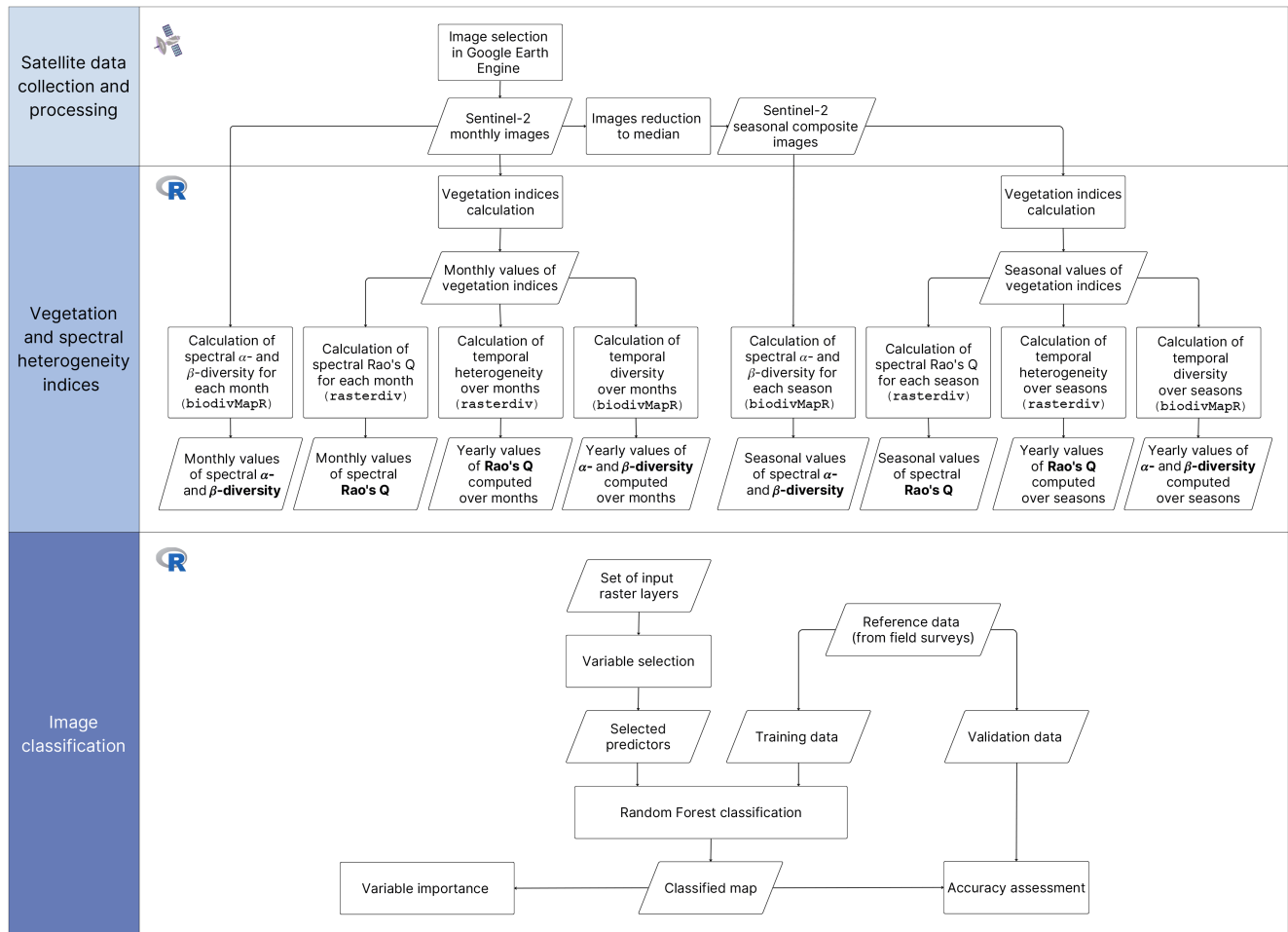


**FIGURE 2** Workflow synthesizing the approach used to map natural habitats through a Random Forest classification and multiple combinations of input layers (vegetation and spectral heterogeneity indices).

**TABLE 1** List of vegetation indices used for the analysis.

Index	Formula	Reference
NDVI	$(NIR_{(B8)} - Red_{(B4)}) / (NIR_{(B8)} + Red_{(B4)})$	Rouse et al. (1975)
GNDVI	$(NIR_{(B8)} - Green_{(B3)}) / (NIR_{(B8)} + Green_{(B3)})$	Gitelson et al. (1996)
NDWI	$(NIR_{(B8)} - SWIR_{(B11)}) / (NIR_{(B8)} + SWIR_{(B11)})$	Chen et al. (2005)
IRECI	$((RedEdge_{(B7)} - Red_{(B4)}) / (RedEdge_{(B5)} / RedEdge_{(B6)})) \times 10000$	Frampton et al. (2013)

Abbreviations: NDVI, Normalized Difference Vegetation Index; GNDVI, Green Normalized Difference Vegetation Index; NDWI, Normalized Difference Water Index; IRECI, Inverted Red-Edge Chlorophyll Index; NIR, Near Infrared; SWIR, Shortwave Infrared.

set of variables was used as input. In the other case, a subset of variables was extracted through recursive feature elimination (RFE; Guyon et al., 2002). The relative variable importance was assessed by the “varImp” function, by systematically comparing the performance of the decision trees that include specific variables and of those that do not, assigning high importance to variables with a positive effect on the prediction accuracy (Breiman, 2001). More details are in Appendix S3.

Accuracy assessment was performed by computing the overall accuracy (OA), the kappa coefficient, the user's accuracy (UA) and the producer's accuracy (PA). After all classifications were

performed, the best classification was repeated using only vegetation indices as input, to assess the effect of excluding SH.

The significance of differences in OA between individual classification pathways was tested with McNemar's test, as suggested by Foody (2004). A t-test was used to assess the effect of choosing 26 or 11 classes on the mean OA, and to compare classifications performed with or without RFE. Finally, differences in mean OA obtained from the four combinations were assessed with a Kruskal-Wallis test.

All classifications and accuracy assessment analyses were performed using R (R Core Team, 2022).

TABLE 2 Sets of input variables used for image classification.

Set of input variables	Input variables	Number of input variables
#1 Monthly aggregated	Vegetation indices: 4 layers per month (NDVI, GNDVI, NDWI, IRECI) Rao's Q: 4 layers per month (NDVI, GNDVI, NDWI, IRECI) $\alpha$ -diversity: 1 layer per month $\beta$ -diversity (first 3 PCoA axes): 3 layers per month	144
#2 Seasonally aggregated	Vegetation indices: 4 layers per season (NDVI, GNDVI, NDWI, IRECI) Rao's Q: 4 layers per season (NDVI, GNDVI, NDWI, IRECI) $\alpha$ -diversity: 1 layer per season $\beta$ -diversity (first 3 PCoA axes): 3 layers per season	48
#3 Yearly aggregated based on monthly values	Temporal Rao's Q: 4 layers per year (NDVI, GNDVI, NDWI, IRECI) Temporal $\alpha$ -diversity: 4 layers per year (NDVI, GNDVI, NDWI, IRECI) Temporal $\beta$ -diversity (first 3 PCoA axes): 3 × 4 layers per year	20
#4 Yearly aggregated based on seasonal values	Temporal Rao's Q: 4 layers per year (NDVI, GNDVI, NDWI, IRECI) Temporal $\alpha$ -diversity: 4 layers per year (NDVI, GNDVI, NDWI, IRECI) Temporal $\beta$ -diversity (first 3 PCoA axes): 3 × 4 layers per year	20

Abbreviations: NDVI, Normalized Difference Vegetation Index; GNDVI, Green Normalized Difference Vegetation Index; NDWI, Normalized Difference Water Index; IRECI, Inverted Red-Edge Chlorophyll Index; PCoA, Principal Coordinate Analysis.

TABLE 3 Overall accuracy (OA) and kappa values obtained from the different classification pathways. Variable selection through recursive feature elimination (RFE) was performed when indicated.

No. of classes	Set of input variables	No. of predictors	OA	Kappa
26	Set #1 (Monthly)	144	0.65	0.58
	Set #1 + RFE	48	0.63	0.56
	Set #2 (Seasonal)	48	0.63	0.56
	Set #2 + RFE	46	0.62	0.54
	Set #3 (Yearly based on months)	20	0.62	0.54
	Set #3 + RFE	20	0.61	0.53
	Set #4 (Yearly based on seasons)	20	0.57	0.50
	Set #4 + RFE	20	0.58	0.51
11	Set #1 (Monthly)	144	0.73	0.65
	Set #1 + RFE	100	0.73	0.65
	Set #1 with only vegetation indices	48	0.69	0.59
	Set #2 (Seasonal)	48	0.72	0.64
	Set #2 + RFE	34	0.72	0.64
	Set #2 with only vegetation indices	16	0.65	0.56
	Set #3 (Yearly based on months)	20	0.66	0.57
	Set #3 + RFE	14	0.67	0.57
	Set #4 (Yearly based on seasons)	20	0.64	0.55
	Set #4 + RFE	17	0.64	0.55

### 3 | RESULTS

#### 3.1 | Accuracy of image classification

The values of OA and kappa obtained from the RF classifications as described in Appendix S3 are in Table 3. The mean OA was significantly higher when 11 habitat classes were considered instead of 26 ( $p$ -value < 0.05; Figure 3a), while there was no significant difference when the number of input variables was reduced through RFE (Figure 3b), nor when different combinations were used as input (Figure 3c).

An OA higher than 70% was achieved only with the monthly and the seasonal combinations, considering 11 habitat classes. For each of these combinations, an additional classification was performed after removing SH layers, and resulted in a lower accuracy (0.65 vs 0.72 for the seasonal combination,  $p$ -value < 0.05; 0.69 vs 0.73 for the monthly combination,  $p$ -value < 0.05).

The classifications that achieved an OA > 70% did not differ significantly among them. Thus, the seasonal combination was chosen as the best one based on a parsimony criterion, for its lower number of predictors (34 predictors after RFE). The habitat map resulting

from this classification is shown in Figure 4: the most common habitats are grassland E2 (24.80%), downy oak woodland (21.70%) and shrubland (16.10%).

The confusion matrix for the best classification is given in Table 4, while class-specific accuracy parameters are in Table 5. The best results were achieved for black pine plantations (PA=0.88, UA=0.92) and downy oak woodland (PA=0.74, UA=0.86), while the lowest values of accuracy were obtained for sessile oak woodlands (UA=0.36, PA=0.27) and invasive alien species groves (UA=0.00, PA=0.00).

In the case of the 26-class classifications, the seasonal combination was also selected as the best one based on a parsimony criterion (OA=0.62; Figure S12). The highest class-specific accuracy (Tables S3 and S4) was found for black pine plantations (UA=0.91, PA=0.89) and the lowest for the two classes of invasive alien species (PA=0.00, UA=0.00). For grassland classes, the different types (mesophilous calcareous, thermophilous calcareous and on flysch) were well differentiated, and most errors occurred between different levels of encroachment and presence of *Sesleria autumnalis*. More details on the class-specific performances are in Appendix S3.

### 3.2 | Relative variable importance

The relative importance of the variables used as input for the best classification is presented in Figure 5. The most important variable

is the principal coordinate 2 (PCo2) of the  $\beta$ -diversity computed from the autumn composite (present in every RF model, equals to 100.00%), followed by PCo1 of the winter  $\beta$ -diversity (94.19%), PCo1 of the autumn  $\beta$ -diversity (88.93%), green normalized difference vegetation index (GNDVI) and inverted red-edge chlorophyll index (IRECI) of the summer (respectively 79.39% and 72.29%).

In the other classifications (Figures S15–S18), the most important variable is almost always  $\beta$ -diversity, with the monthly classification with 11 classes as the only exception, in which vegetation indices are at the first places. The relative importance of the indices of  $\alpha$ -diversity and Rao's Q is low in all the classifications: the maximum values are respectively 42.56% for  $\alpha$ -diversity (in the monthly 26-classes classification) and 64.91% for Rao's Q (in the monthly 11-classes classification). A description of the input variables is given in Appendix S2.

## 4 | DISCUSSION

The approach developed in this study showed the potential of novel SH indices and multitemporal frameworks for the automatic mapping of vegetation types in complex landscapes. In our example, the landscape was highly dynamic and our goal was to develop a framework to classify vegetation types with a high level of detail, to monitor their distribution and to assess the effects of management over different areas and in short periods of

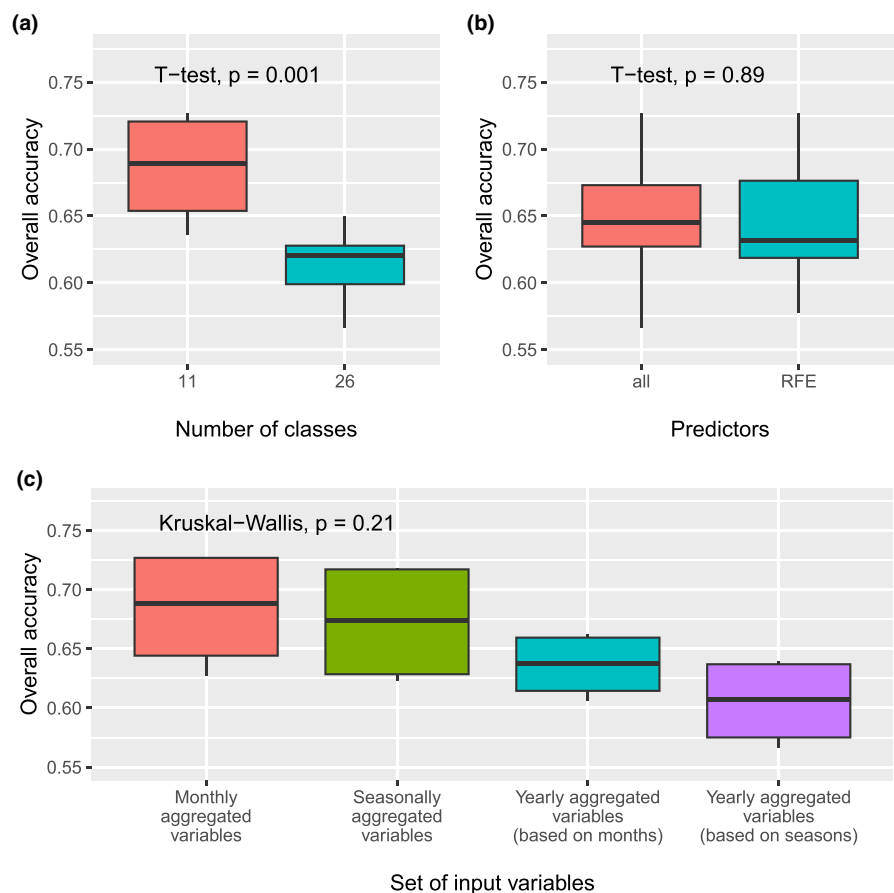
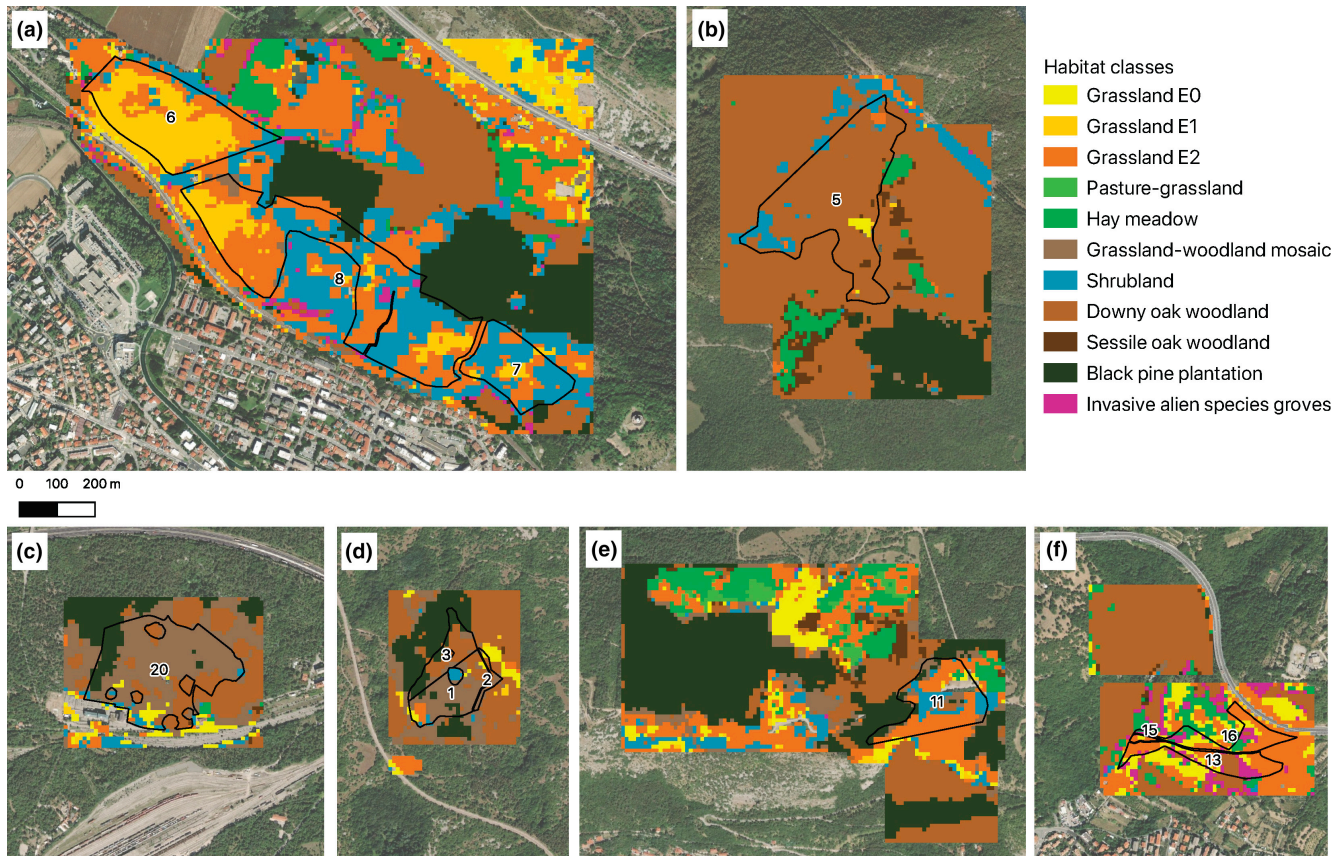


FIGURE 3 Comparison of the overall accuracy achieved by (a) considering different numbers of habitat classes; (b) by performing or not a variable selection step through recursive feature elimination (RFE); and (c) by using different input combinations.



**FIGURE 4** Habitat map resulting from the Random Forest classification based on seasonal layers of vegetation and spectral heterogeneity indices. Among all the possible classifications, the one selected is the one that resulted in the highest accuracy while minimizing the number of input layers. A total of 11 habitat classes was considered, based on structural-physiognomic and ecological characteristics. The areas are located in Monfalcone (a), Case Coisce (b), Opicina (c), Aurisina (d), San Lorenzo (e) and San Giuseppe (f).

**TABLE 4** Confusion matrix for the best classification (seasonal classification performed with 11 classes).

	Gr_E0	Gr_E1	Gr_E2	PG	HM	GWM	Shr	DOW	SOW	BPP	IAS
Gr_E0	12							2			1
Gr_E1		21	5				1				
Gr_E2	3	7	51	1	2	3	1	5	1		
PG				1							
HM				6	10			1			
GWM	2	1	2		1	13	1	22		4	
Shr		2	20				8	6		1	2
DOW			1		1	1	2	156	10	9	1
SOW								7	4		
BPP						1	1	7		107	
IAS			1					4		1	

*Note:* The rows represent the results obtained from the classification, while the columns represent the reference data. The values on the matrix diagonal, highlighted with gray shades, are the correctly classified pixels. Abbreviations: Gr\_E0, grassland with no encroachment; Gr\_E1, grassland at first encroachment stage; Gr\_E2, grassland at second encroachment stage; PG, pasture grassland; HM, hay meadow; GWM, grassland-woodland mosaic; Shr, shrubland; DOW, downy oak woodland; SOW, sessile oak woodland; BPP, black pine plantation; IAS, invasive alien species.

time. In this context, remote sensing allowed the development of time-effective and efficient monitoring strategies, even if the maximum level of accuracy achievable was likely constrained by the presence of transition areas with high heterogeneity, by the

spatial and spectral resolution of satellite data, and by the presence of some classes particularly difficult to map and with small patches. Nonetheless, remote sensing provides a useful basis, for example to identify sites with potential for restoration (Marignani



et al., 2008), that can be improved with more detailed field analysis on limited areas.

#### 4.1 | Accuracy of image classifications

In this study, multiple RF classifications were performed to test different combinations of vegetation and SH indices, using as study area a complex mosaic of habitats in the Classical Karst. The small spatial extent of the habitat patches, their spectral similarity and the high variability of vegetation make this type of landscape challenging to map from remote sensing (Tarantino et al., 2021). The maximum OA achieved in this study (0.73) is comparable to the levels of accuracy achieved by similar studies. Rapinel et al. (2019) mapped seven wet grassland plant communities with an accuracy of 0.78, using Sentinel-2 time series. Tarantino et al. (2021) achieved an

accuracy of 0.95 using multiseasonal Sentinel-2 images, a time series of the modified soil adjusted vegetation index (MSAVI) and a digital terrain model (DTM), but they only mapped four grassland types. Bhatt et al. (2022), who used very high-resolution imagery (60 cm) to map nine heterogeneous habitats, reached an accuracy of 0.79.

In this study, habitat classes were defined with a high level of detail. Although the high number of classes reduced the accuracy of image classifications (maximum OA=0.65 for the 26-class classifications, as shown in Figure 3a), our approach was promising, because it allowed differentiation of the types of grassland, distinction of patches of typical grasslands from patches completely invaded by *Sesleria autumnalis*, and differentiation of the earliest stages of encroachment from the most advanced ones. The conservation of grassland depends on the persistence of the typical species (Butaye et al., 2005) and on the degree of encroachment (Altobelli et al., 2014); thus, distinguishing the transitional stages of grassland by remote sensing is highly important for conservation.

Two other factors increased the complexity of the classification. Firstly, the intra-habitat variability was high in the study area due to differences in altitude and substrate composition (Poldini, 1989). Generally, spectrally heterogeneous habitats are more difficult to map (Villoslada et al., 2020), and indeed we observed the best performances for black pine plantations, the most spectrally homogeneous habitats. Secondly, most habitat patches were small (median patch size=0.32 ha, 20% of the patches covering less than 10 pixels), thus the proportion of mixed pixels was high, complicating habitat separation (Rocchini et al., 2013). The lowest class-specific accuracy, indeed, was found for invasive alien species groves that were present in the smallest areas. In our case, *Ailanthus altissima* and *Robinia pseudoacacia* stands were considered as a single habitat class (i.e. Invasive Alien Species), but the two species might have a different spectral signature, and this could explain the low accuracy in classifying this habitat class. The use of hyperspectral imagery could facilitate the differentiation of target alien species and lead to more promising results (Rocchini et al., 2015).

TABLE 5 Class-specific accuracy parameters obtained for the seasonal classification performed with 11 classes. Accuracy was assessed using independent validation data.

Class	UA	PA
Grassland E0	0.80	0.71
Grassland E1	0.78	0.68
Grassland E2	0.69	0.64
Pasture-grassland	1.00	0.13
Hay meadow	0.59	0.71
Grassland-woodland mosaic	0.28	0.72
Shrubland	0.21	0.57
Downy oak woodland	0.86	0.74
Sessile oak woodland	0.36	0.27
Black pine plantation	0.92	0.88
Invasive alien species groves	0.00	0.00

Abbreviations: UA, user's accuracy; PA, producer's accuracy.

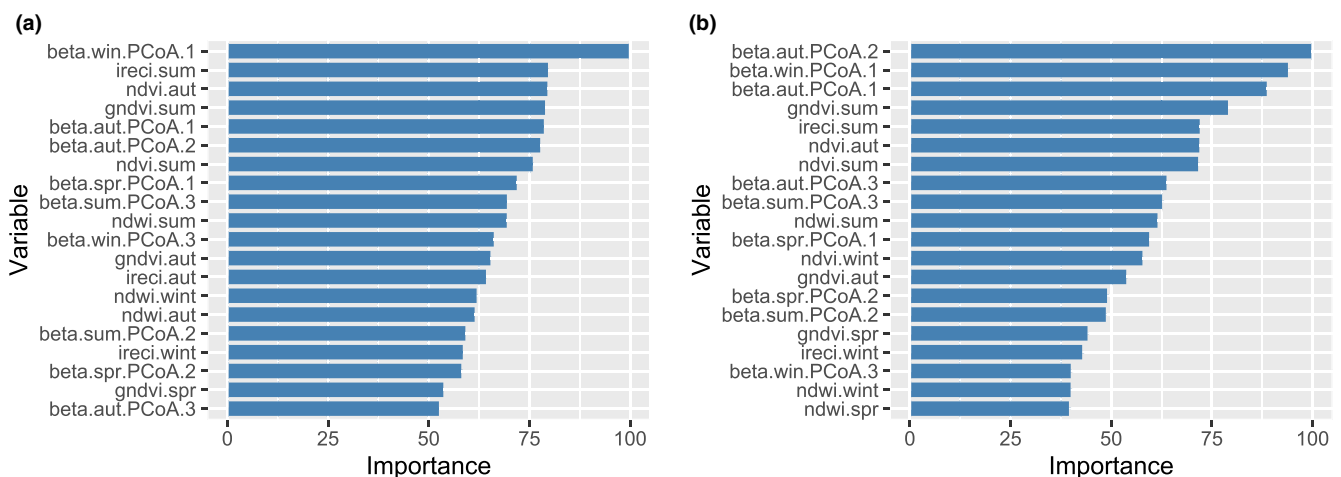


FIGURE 5 Relative importance of the variables used as input for the seasonal classifications with 11 classes. Classifications were performed with the whole set of input variables (a) and with a subset obtained by RFE (b). Only the first 20 variables are shown.

SH measures improved the capacity of classifying habitats from satellite data. The classifications performed without SH measures (maximum OA=0.69) were significantly less accurate than the others (maximum OA=0.73), and the resulting maps were more confused, as the spatial integrity of the classes was not maintained. SH is mainly investigated nowadays for its relationship with species richness (Wang & Gamon, 2019), and it has rarely been used for the classification of habitats. Our results suggest that image classification frameworks could benefit from the inclusion of SH measures as an additional level of information, although with differences according to the type of metric.

The most important variable in almost all the classifications was spectral  $\beta$ -diversity, defined here based on the spectral species approach (Féret & Asner, 2014). All diversity metrics based on this approach have some advantages. The distinction of spectral species is based on k-means clustering, which exploits the full spectral information (Féret & Asner, 2014), and groups spectrally extreme pixels into separate classes, avoiding an unproportional effect on the results (Fassnacht et al., 2022). Moreover, the algorithm involves two ordinations, an initial principal components analysis (PCA) and a principal coordinates analysis (PCoA) for the computation of spectral  $\beta$ -diversity, that are useful to reduce feature dimensionality while maximizing spectral separability (Borra et al., 2019). Although both  $\alpha$ - and  $\beta$ -diversity in this study were based on the same approach, the latter was far more important than the former for habitat classification. Indeed,  $\beta$ -diversity allows habitats to be differentiated based on their compositional dissimilarity, while a similar  $\alpha$ -diversity can be shared also by habitats with different species (Whittaker, 1960). Here, spectral  $\beta$ -diversity clearly separated the three main groups of habitats in the Classical Karst: habitats dominated by woody deciduous plants (woodlands and shrublands), habitats dominated by herbaceous plants (grasslands and meadows) and habitats dominated by evergreens (pine forests).

Moreover, the link between species and spectral diversity seems to be stronger for  $\beta$ - than for  $\alpha$ -diversity. In many studies,  $\alpha$ -diversity could only be estimated with very high-resolution data (e.g. 1 m<sup>2</sup> in Wang et al., 2016), while  $\beta$ -diversity could be estimated also at coarser spatial resolutions (e.g. 20×50m in Rocchini, He, et al., 2010), although generally less studies focused on this component (Wang & Gamon, 2019).

The other SH index considered in this study, spectral Rao's Q, had a low relative importance. This index measures the heterogeneity of a pixel with respect to its surroundings (Thouverai et al., 2021), and matches species diversity in natural areas but not in heterogeneous agricultural lands (Rocchini, Salvatori, et al., 2021). We found an unclear relation between spectral Rao's Q and species diversity: the lowest Rao's Q values were found for black pine plantations, which host a low species diversity, and the highest values for pasture grasslands and pure grasslands, which are species-rich habitats (Poldini, 2009), but high values were found unexpectedly also for invasive alien species groves. One possible reason is the spatial extent of the habitat patches: habitats with smaller patches are more likely to border with different habitats inside the moving window used to

calculate the index, and thus to have higher Rao's Q values. Using data with higher spatial resolution would probably improve this aspect. However, the approach used to calculate Rao's Q may itself be a problem, since it highlights the differences among close pixels, and thus maximizes the noise, instead of minimizing it. Therefore, while the Rao's Q index can be used to estimate species diversity in some cases (Rocchini, Salvatori, et al., 2021), it might be less useful in the context of habitat mapping.

Our results show that some SH metrics might be more useful than others for habitat mapping. These measures can be useful regardless of their link with actual species diversity, which is still often unclear, since they allow the exploitation of the main strength of remote sensing: repeating measures over time, to capture habitat-specific variations and monitor landscape evolution (Fassnacht et al., 2022).

## 4.2 | Importance of vegetation indices

Vegetation indices were the most important variables after  $\beta$ -diversity in all the monthly and seasonal classifications. In particular, summer GNDVI and IRECI and autumn NDVI were the most important vegetation indices in the best classification. NDVI, with its variant GNDVI, has been found useful in many studies (e.g. Schuster et al., 2015).

IRECI is the only index considered that includes the Red Edge Sentinel-2 bands and has a strong linear relationship with canopy chlorophyll content and leaf area index (LAI) (Frampton et al., 2013). Here, IRECI varies following the seasonal changes of canopy chlorophyll content, with an increase in spring, a maximum in summer and a decrease in autumn (Gara et al., 2019). Differences between habitats reflect the differences in chlorophyll content between broadleaved trees and conifers (Li et al., 2018) and the differences in LAI across ecosystems, which generally increases from grasslands and shrublands to temperate deciduous broadleaved and evergreen needle-leaved forests (Asner et al., 2003). Optical traits like chlorophyll content can improve the estimation and mapping of species composition over space, as demonstrated by Feilhauer et al. (2017) in semi-natural temperate grasslands. Although IRECI itself has not been tested much for habitat mapping, other indices using the Red Edge spectrum have been shown to be useful. For example, Schuster et al. (2012) found that the Red Edge channel of the RapidEye satellite had a positive influence on the overall accuracy of a land cover classification in a mosaic of natural and agricultural areas in Germany, especially for the bush and dry grassland classes. Bayle et al. (2019) distinguished alpine grasslands from shrublands relying on the Sentinel-2 Red Edge bands, by detecting the seasonal anthocyanin accumulation in the shrub species. A Red Edge-based index was also found to be more useful than NDVI to map plant communities in coastal meadows (Villoslada et al., 2020). These examples are in line with our results, which confirm the role of the Red Edge spectrum for the distinction of habitats.

### 4.3 | Inclusion of multitemporal data

The aggregation of monthly data in seasonal composites using the median statistical operator allowed the reduction of the number of input layers without losing information. The levels of accuracy achieved with the monthly and seasonal combinations were, indeed, not significantly different, while the number of input layers was reduced from 144 to 48. This method of reducing data dimensionality can be complemented with variable selection through RFE, which did not have a significant effect on accuracy (as shown in Figure 3b). The use of seasonal composites for habitat mapping is known to be useful because it reduces the problem of cloudy images but maintains the advantage given by multitemporal data (Kollert et al., 2021). In a recent work by Praticò et al. (2021), the mean turned out to produce slightly better results than other statistical operators such as the median. In this study the median was chosen because it is less sensitive to outliers and is the most common way to perform image reduction (Kollert et al., 2021), but other statistical operators could be investigated.

The combinations including only yearly aggregated values of spectral diversity and heterogeneity generally led to worse results than the other combinations (mean OA=0.59 for 26 classes and 0.65 for 11 classes, Figure 3c). Marzialetti et al. (2020) achieved good results using the temporal Rao's Q of vegetation indices computed over a year to map coastal dune habitats, but they included also the mean, the 10th and the 90th percentiles of vegetation indices. Here, only temporal heterogeneity layers were used, thus including other measures that summarize the annual variation of vegetation indices could increase the capacity of distinguishing habitats.

The most relevant seasons for distinguishing vegetation types in the Classical Karst were summer, autumn and winter, but spring was also important in some classifications, suggesting that there is not one single period better than the others, and confirming the advantage of using multitemporal data (e.g. Schuster et al., 2015; Rapinel et al., 2019). Each season can provide specific information, as was found for example by Soubry and Guo (2021) to distinguish shrubs and grasslands: in spring the most important feature was the peak in growth (red and blue bands), in summer the leaf structure (near infrared bands), while in autumn the greenness and moisture (shortwave infrared and red bands). In the case of Classical Karst, autumn and winter generally allowed evergreens to be distinguished from deciduous or semi-deciduous plants, while summer separated the different deciduous forest habitats especially with the NDVI and IRECI indices.

## 5 | CONCLUSIONS

In this study, we tested novel SH indices in a multitemporal classification framework and demonstrated their potential to improve habitat mapping in complex landscapes, using the Classical Karst as testing area.

Our framework could be improved using different remote-sensing data sources, as hyperspectral sensors, sensors with higher spatial resolutions, or active sensors (Nagendra et al., 2013). Moreover, other combinations of input variables can possibly produce better results, such as combinations of Sentinel-1 and Sentinel-2 time series (Fauvel et al., 2020).

The framework presented here was applied to some areas of the Classical Karst, but could be extended to test its validity on a larger scale. This approach based on remote sensing cannot replace field work and requires field data for training and validation, though it can be a valid tool to map habitats in a cost- and time-effective way that is very suitable for monitoring purposes.

### AUTHOR CONTRIBUTIONS

Emilia Pafumi, Francesco Petruzzellis and Giovanni Bacaro conceived the study, with additional input from Miris Castello and Alfredo Altobelli; Emilia Pafumi, Francesco Petruzzellis and Miris Castello collected the data; Emilia Pafumi and Francesco Petruzzellis performed the analysis, with contributions from the other authors for the interpretation of the results; Emilia Pafumi wrote the first draft; Francesco Petruzzellis, Giovanni Bacaro, Miris Castello, Simona Maccherini and Duccio Rocchini contributed to the writing; all authors critically revised the manuscript and gave final approval for publication.

### FUNDING INFORMATION

This study was conducted within the "Ecomosaico del Carso" project, funded by the Rural Development Program (Programma di Sviluppo Rurale) 2014–2020 of Friuli Venezia Giulia Region. Authors who received this funding are Alfredo Altobelli, Emilia Pafumi, Giovanni Bacaro, and Miris Castello. Francesco Petruzzellis is currently supported by the funding PON Ricerca e Innovazione D.M. 1062/21–Contratti di ricerca, from the Italian Ministry of University (MUR).

### CONFLICT OF INTEREST STATEMENT

The authors have no conflict of interest to declare.

### DATA AVAILABILITY STATEMENT

The Sentinel-2 images can be downloaded from the Google Earth Engine platform. All analysis tools can be found in the R packages cited in the manuscript. The reference data set and the R script used for image classifications are available in the electronic Supplementary Information.

### ORCID

Emilia Pafumi  <https://orcid.org/0000-0003-1592-1964>

Francesco Petruzzellis  <https://orcid.org/0000-0002-3635-8501>

Miris Castello  <https://orcid.org/0000-0002-5081-0365>

Alfredo Altobelli  <https://orcid.org/0000-0002-4038-7014>

Simona Maccherini  <https://orcid.org/0000-0002-2025-7546>

Duccio Rocchini  <https://orcid.org/0000-0003-0087-0594>

Giovanni Bacaro  <https://orcid.org/0000-0003-0946-4496>

## REFERENCES

- Altobelli, A., Ganis, P., Zanatta, K. & Zanetti, M. (2014) Processing of images obtained using UAV/RPAS to assess the degree of scrubbing over dry grasslands in the Gorizian karst. In: Buzan, E. & Pallavicini, A. (Eds.) *Biodiversity and conservation of karst ecosystems*. Padua: Padova University Press, pp. 155–164.
- Asner, G.P., Scurlock, J.M.O. & Hicke, J.A. (2003) Global synthesis of leaf area index observations: implications for ecological and remote sensing studies: global leaf area index. *Global Ecology and Biogeography*, 12, 191–205. Available from: <https://doi.org/10.1046/j.1466-822X.2003.00026.x>
- Bayle, A., Carlson, B., Thierion, V., Isenmann, M. & Choler, P. (2019) Improved mapping of mountain Shrublands using the Sentinel-2 red-edge band. *Remote Sensing*, 11, 2807. Available from: <https://doi.org/10.3390/rs11232807>
- Bhatt, P., Maclean, A., Dickinson, Y. & Kumar, C. (2022) Fine-scale mapping of natural ecological communities using machine learning approaches. *Remote Sensing*, 14, 563. Available from: <https://doi.org/10.3390/rs14030563>
- Borra, S., Thanki, R. & Dey, N. (2019) *Satellite image analysis: clustering and classification*. SpringerBriefs in applied sciences and technology. Singapore: Springer Singapore.
- Breiman, L. (2001) Random forests. *Machine Learning*, 45, 5–32. Available from: <https://doi.org/10.1023/A:1010933404324>
- Butaye, J., Adriaens, D. & Honnay, O. (2005) Conservation and restoration of calcareous grasslands: a concise review of the effects of fragmentation and management on plant species. *Biotechnology, Agronomy, Society and Environment*, 9, 111–118.
- Chen, D., Huang, J. & Jackson, T.J. (2005) Vegetation water content estimation for corn and soybeans using spectral indices derived from MODIS near- and short-wave infrared bands. *Remote Sensing of Environment*, 98, 225–236. Available from: <https://doi.org/10.1016/j.rse.2005.07.008>
- Chraïbi, E., Arnold, H., Luque, S., Deacon, A., Magurran, A. & Féret, J.-B. (2021) A remote sensing approach to understanding patterns of secondary succession in tropical Forest. *Remote Sensing*, 13, 2148. Available from: <https://doi.org/10.3390/rs13112148>
- Corbane, C., Lang, S., Pipkins, K., Alleaume, S., Deshayes, M., García Millán, V.E. et al. (2015) Remote sensing for mapping natural habitats and their conservation status – new opportunities and challenges. *International Journal of Applied Earth Observation and Geoinformation, Special Issue on Earth Observation for Habitat Mapping and Biodiversity Monitoring*, 37, 7–16. Available from: <https://doi.org/10.1016/j.jag.2014.11.005>
- European Commission. (1992) *Council Directive 92/43/EEC of 21 May 1992 on the conservation of natural habitats and of wild fauna and flora* (OJ L 206 22.07.1992 p. 7).
- European Commission. (2005) *Note to the habitats committee. Assessment, monitoring and reporting of conservation status – preparing the 2001–2007 report under article 17 of the habitats directive* (No. DocHab-04-03/03 rev.3). Brussels: European Commission.
- Fassnacht, F.E., Müllerová, J., Conti, L., Malavasi, M. & Schmidlein, S. (2022) About the link between biodiversity and spectral variation. *Applied Vegetation Science*, 25, e12643. Available from: <https://doi.org/10.1111/avsc.12643>
- Fauvel, M., Lopes, M., Dubo, T., Rivers-Moore, J., Frison, P.-L., Gross, N. et al. (2020) Prediction of plant diversity in grasslands using Sentinel-1 and -2 satellite image time series. *Remote Sensing of Environment*, 237, 111536. Available from: <https://doi.org/10.1016/j.rse.2019.111536>
- Feilhauer, H., Somers, B. & van der Linden, S. (2017) Optical trait indicators for remote sensing of plant species composition: predictive power and seasonal variability. *Ecological Indicators*, 73, 825–833. Available from: <https://doi.org/10.1016/j.ecolind.2016.11.003>
- Féret, J.-B. & Asner, G.P. (2014) Mapping tropical forest canopy diversity using high-fidelity imaging spectroscopy. *Ecological Applications*, 24, 1289–1296. Available from: <https://doi.org/10.1890/13-1824.1>
- Féret, J.-B. & de Boissieu, F. (2020) biodivMapR: an R package for  $\alpha$ - and  $\beta$ -diversity mapping using remotely sensed images. *Methods in Ecology and Evolution*, 11, 64–70. Available from: <https://doi.org/10.1111/2041-210X.13310>
- Foody, G.M. (2004) Thematic map comparison: evaluating the statistical significance of differences in classification accuracy. *Photogrammetric Engineering & Remote Sensing*, 70, 627–633. Available from: <https://doi.org/10.14358/PERS.70.5.627>
- Frampton, W.J., Dash, J., Watmough, G. & Milton, E.J. (2013) Evaluating the capabilities of Sentinel-2 for quantitative estimation of biophysical variables in vegetation. *ISPRS Journal of Photogrammetry and Remote Sensing*, 82, 83–92. Available from: <https://doi.org/10.1016/j.isprsjprs.2013.04.007>
- Gara, T.W., Darvishzadeh, R., Skidmore, A.K., Wang, T. & Heurich, M. (2019) Accurate modelling of canopy traits from seasonal Sentinel-2 imagery based on the vertical distribution of leaf traits. *ISPRS Journal of Photogrammetry and Remote Sensing*, 157, 108–123. Available from: <https://doi.org/10.1016/j.isprsjprs.2019.09.005>
- Gitelson, A.A., Kaufman, Y.J. & Merzlyak, M.N. (1996) Use of a green channel in remote sensing of global vegetation from EOS-MODIS. *Remote Sensing of Environment*, 58, 289–298. Available from: [https://doi.org/10.1016/S0034-4257\(96\)00072-7](https://doi.org/10.1016/S0034-4257(96)00072-7)
- Gorelick, N., Hancher, M., Dixon, M., Ilyushchenko, S., Thau, D. & Moore, R. (2017) Google Earth Engine: planetary-scale geospatial analysis for everyone. *Remote Sensing of Environment*, 202, 18–27. Available from: <https://doi.org/10.1016/j.rse.2017.06.031>
- Guyon, I., Weston, J., Barnhill, S. & Vapnik, V. (2002) Gene selection for cancer classification using support vector machines. *Machine Learning*, 46, 389–422. Available from: <https://doi.org/10.1023/A:1012487302797>
- Haralick, R.M., Shanmugam, K. & Dinstein, I. (1973) Textural features for image classification. *IEEE Transactions on Systems, Man, and Cybernetics*, SMC-3, 610–621. Available from: <https://doi.org/10.1109/TSMC.1973.4309314>
- Khatami, R., Mountrakis, G. & Stehman, S.V. (2016) A meta-analysis of remote sensing research on supervised pixel-based land-cover image classification processes: general guidelines for practitioners and future research. *Remote Sensing of Environment*, 177, 89–100. Available from: <https://doi.org/10.1016/j.rse.2016.02.028>
- Kollert, A., Bremer, M., Löw, M. & Rutzinger, M. (2021) Exploring the potential of land surface phenology and seasonal cloud free composites of one year of Sentinel-2 imagery for tree species mapping in a mountainous region. *International Journal of Applied Earth Observation and Geoinformation*, 94, 102208. Available from: <https://doi.org/10.1016/j.jag.2020.102208>
- Kuhn, M. (2021) *Caret: classification and regression training*. R package version 6.0-90. Available from: <https://CRAN.R-project.org/package=caret>
- Li, Y., He, N., Hou, J., Xu, L., Liu, C., Zhang, J. et al. (2018) Factors influencing leaf chlorophyll content in natural forests at the biome scale. *Frontiers in Ecology and Evolution*, 6, 64. Available from: <https://doi.org/10.3389/fevo.2018.00064>
- Liccardi, F., Sigura, M. & Bacaro, G. (2022) Use of remote sensing techniques to estimate plant diversity within ecological networks: a worked example. *Remote Sensing*, 14, 4933. Available from: <https://doi.org/10.3390/rs14194933>
- Marignani, M., Rocchini, D., Torri, D., Chiarucci, A. & Maccherini, S. (2008) Planning restoration in a cultural landscape in Italy using an object-based approach and historical analysis. *Landscape and Urban Planning*, 84, 28–37. Available from: <https://doi.org/10.1016/j.landurbplan.2007.06.005>

- Marin, A. & Altobelli, A. (2021) Social ecology and traditional landscape enhancement. Some issues from a case study in the Gorizia karst. *SMC Magazine*, 5, 55–60.
- Marzialetti, F., Di Febraro, M., Malavasi, M., Giulio, S., Acosta, A.T.R. & Carranza, M.L. (2020) Mapping coastal dune landscape through spectral Rao's Q temporal diversity. *Remote Sensing*, 12, 2315. Available from: <https://doi.org/10.3390/rs12142315>
- Nagendra, H., Lucas, R., Honrado, J.P., Jongman, R.H.G., Tarantino, C., Adamo, M. et al. (2013) Remote sensing for conservation monitoring: assessing protected areas, habitat extent, habitat condition, species diversity, and threats. *Ecological Indicators, Biodiversity Monitoring*, 33, 45–59. Available from: <https://doi.org/10.1016/j.ecolind.2012.09.014>
- Osińska-Skotak, K., Radecka, A., Ostrowski, W., Michalska-Hejduk, D., Charyton, J., Bakuła, K. et al. (2021) The methodology for identifying secondary succession in non-Forest Natura 2000 habitats using multi-source airborne remote sensing data. *Remote Sensing*, 13, 2803. Available from: <https://doi.org/10.3390/rs13142803>
- OSMER. (2015) *Schede climatiche territoriali del Friuli Venezia Giulia*. ARPA FVG. Available from: [https://www.clima.fvg.it/clima\\_schede.php?m=1](https://www.clima.fvg.it/clima_schede.php?m=1) [Accessed 20th May 2022].
- Palmer, M.W., Earls, P.G., Hoagland, B.W., White, P.S. & Wohlgemuth, T. (2002) Quantitative tools for perfecting species lists. *Environmetrics*, 13, 121–137. Available from: <https://doi.org/10.1002/env.516>
- Poldini, L. (1989) *The vegetation of the Trieste and Isonzo karst: study of the plant landscape between Trieste, Gorizia and the adjacent territories* (Italian). Trieste: Lint. ed.
- Poldini, L. (2009) *The plant diversity of the karst between Trieste and Gorizia: the state of the environment* (Italian). Trieste: Ed. Goliardiche.
- Praticò, S., Solano, F., Di Fazio, S. & Modica, G. (2021) Machine learning classification of Mediterranean Forest habitats in Google earth engine based on seasonal Sentinel-2 time-series and input image composition optimisation. *Remote Sensing*, 13, 586. Available from: <https://doi.org/10.3390/rs13040586>
- QGIS Development Team. (2022) *QGIS geographic information system*. Available from: <http://www.qgis.org>
- R Core Team. (2022) *R: a language and environment for statistical computing*. Vienna: R Foundation for Statistical Computing. Available from: <https://www.R-project.org/>
- Rapinel, S., Mony, C., Lecoq, L., Clément, B., Thomas, A. & Hubert-Moy, L. (2019) Evaluation of Sentinel-2 time-series for mapping flood-plain grassland plant communities. *Remote Sensing of Environment*, 223, 115–129. Available from: <https://doi.org/10.1016/j.rse.2019.01.018>
- Rocchini, D., Andreo, V., Förster, M., Garzon-Lopez, C.X., Gutierrez, A.P., Gillespie, T.W. et al. (2015) Potential of remote sensing to predict species invasions: a modelling perspective. *Progress in Physical Geography: Earth and Environment*, 39, 283–309. Available from: <https://doi.org/10.1177/0309133315574659>
- Rocchini, D., Balkenhol, N., Carter, G.A., Foody, G.M., Gillespie, T.W., He, K.S. et al. (2010) Remotely sensed spectral heterogeneity as a proxy of species diversity: recent advances and open challenges. *Ecological Informatics*, 5, 318–329. Available from: <https://doi.org/10.1016/j.ecoinf.2010.06.001>
- Rocchini, D., Foody, G.M., Nagendra, H., Ricotta, C., Anand, M., He, K.S. et al. (2013) Uncertainty in ecosystem mapping by remote sensing. *Computers & Geosciences*, 50, 128–135. Available from: <https://doi.org/10.1016/j.cageo.2012.05.022>
- Rocchini, D., He, K.S., Oldeland, J., Wesuls, D. & Neteler, M. (2010) Spectral variation versus species  $\beta$ -diversity at different spatial scales: a test in African highland savannas. *Journal of Environmental Monitoring*, 12, 825–831. Available from: <https://doi.org/10.1039/b921835a>
- Rocchini, D., Marcantonio, M., Da Re, D., Bacaro, G., Feoli, E., Foody, G.M. et al. (2021) From zero to infinity: minimum to maximum diversity of the planet by spatio-parametric Rao's quadratic entropy. *Global Ecology and Biogeography*, 30, 1153–1162. Available from: <https://doi.org/10.1111/geb.13270>
- Rocchini, D., Salvatori, N., Beierkuhnlein, C., Chiarucci, A., de Boissieu, F., Förster, M. et al. (2021) From local spectral species to global spectral communities: a benchmark for ecosystem diversity estimate by remote sensing. *Ecological Informatics*, 61, 101195. Available from: <https://doi.org/10.1016/j.ecoinf.2020.101195>
- Rossi, C., Kneubühler, M., Schütz, M., Schaeppman, M.E., Haller, R.M. & Risch, A.C. (2021) Spatial resolution, spectral metrics and biomass are key aspects in estimating plant species richness from spectral diversity in species-rich grasslands. *Remote Sensing in Ecology and Conservation*, 8, 297–314. Available from: <https://doi.org/10.1002/rse2.244>
- Rouse, J.W., Haas, R.H. & Schell, J.A.W. (1975) *Monitoring vegetation systems in the great plains with ERTS*. Presented at the Third ERTS Symposium.
- Schuster, C., Förster, M. & Kleinschmit, B. (2012) Testing the red edge channel for improving land-use classifications based on high-resolution multi-spectral satellite data. *International Journal of Remote Sensing*, 33, 5583–5599. Available from: <https://doi.org/10.1080/01431161.2012.666812>
- Schuster, C., Schmidt, T., Conrad, C., Kleinschmit, B. & Förster, M. (2015) Grassland habitat mapping by intra-annual time series analysis – comparison of RapidEye and TerraSAR-X satellite data. *International Journal of Applied Earth Observation and Geoinformation*, 34, 25–34. Available from: <https://doi.org/10.1016/j.jag.2014.06.004>
- Soubry, I. & Guo, X. (2021) Identification of the optimal season and spectral regions for shrub cover estimation in grasslands. *Sensors*, 21, 3098. Available from: <https://doi.org/10.3390/s21093098>
- Tarantino, C., Forte, L., Blonda, P., Vicario, S., Tomaselli, V., Beierkuhnlein, C. et al. (2021) Intra-annual Sentinel-2 time-series supporting grassland habitat discrimination. *Remote Sensing*, 13, 277. Available from: <https://doi.org/10.3390/rs13020277>
- Thouverai, E., Marcantonio, M., Bacaro, G., Da Re, D., Iannacito, M., Marchetto, E. et al. (2021) Measuring diversity from space: a global view of the free and open source rasterdiv R package under a coding perspective. *Community Ecology*, 22, 1–11. Available from: <https://doi.org/10.1007/s42974-021-00042-x>
- Villoslada, M., Bergamo, T.F., Ward, R.D., Burnside, N.G., Joyce, C.B., Bunce, R.G.H. et al. (2020) Fine scale plant community assessment in coastal meadows using UAV based multispectral data. *Ecological Indicators*, 111, 105979. Available from: <https://doi.org/10.1016/j.ecolind.2019.105979>
- Wang, R., Gamon, J., Emmerton, C., Li, H., Nestola, E., Pastorello, G. et al. (2016) Integrated analysis of productivity and biodiversity in a southern Alberta prairie. *Remote Sensing*, 8, 214. Available from: <https://doi.org/10.3390/rs8030214>
- Wang, R. & Gamon, J.A. (2019) Remote sensing of terrestrial plant biodiversity. *Remote Sensing of Environment*, 231, 111218. Available from: <https://doi.org/10.1016/j.rse.2019.111218>
- Wang, R., Gamon, J.A., Cavender-Bares, J., Townsend, P.A. & Zyguelbaum, A.I. (2018) The spatial sensitivity of the spectral diversity–biodiversity relationship: an experimental test in a prairie grassland. *Ecological Applications*, 28, 541–556. Available from: <https://doi.org/10.1002/eap.1669>
- Whittaker, R.H. (1960) Vegetation of the Siskiyou Mountains, Oregon and California. *Ecological Monographs*, 30, 279–338. Available from: <https://doi.org/10.2307/1943563>

## SUPPORTING INFORMATION

Additional supporting information can be found online in the Supporting Information section at the end of this article.

**Appendix S1.** Study area and habitat classes.

**Appendix S2.** Vegetation and SH indices.

**Appendix S3.** Satellite image classifications.

Data S1.

**How to cite this article:** Pafumi, E., Petruzzellis, F., Castello, M., Altobelli, A., Maccherini, S., Rocchini, D. et al. (2023) Using spectral diversity and heterogeneity measures to map habitat mosaics: An example from the Classical Karst. *Applied Vegetation Science*, 26, e12762. Available from: <https://doi.org/10.1111/avsc.12762>